JET-P(96)12

Toroidicity in the Tokamak SOL: Effects on Poloidal Asymmetries, Radial Current and the L-H Transition

A V Chankin[1], P C Stangeby[2].

JET Joint Undertaking, Abingdon, Oxfordshire, OX14 3EA, UK.
[1] Permanent Address: Russian Scientific Centre "Kurchatov Institute", INF Moscow, Russia.
[2] Permanent Address: University of Toronto Institute for Aerospace Studies, Ontario, Canada, M3H 5T6.

Preprint of a paper to be submitted for application in Plasma Physics and Controlled Fusion

April 1996

ABSTRACT

A simple isothermal model for the scrape-off layer (SOL) which includes effects of toroidal geometry and radial electric field, but ignores viscosity and plasma-neutral interactions, is presented. For finite toroidicity $\varepsilon = a/R$, and for the case of zero radial electric field E_r, the model predicts pressure asymmetry in favour of the outer target, and a non-zero radial current j_r due to pressure gradient terms. For the case of non-zero E_r, j_r is changed somewhat. The dependence of the current on the radial electric field, however, is too weak and non-monotonic against E_r, to explain experimental results on ion mobility obtained in biasing experiments on the Tokamak de Varennes. This may indicate that anomalous processes, not considered here, are controlling in TdeV. The direction of the pressure gradient driven current is inwards for "normal" toroidal field (ion ∇B drift towards the single null divertor), and outwards - for the "reversed" field. The current can cause significant changes in radial flux in the SOL between the two field directions, for the case when the SOL width approaches the ion poloidal Larmor radius. Its effect on the SOL is proposed as a mechanism responsible for the dependence of the threshold power, needed to cause the L-H transition, on the direction of the toroidal field. The dependence of the current on the toroidicity: $j_r \sim \varepsilon^{\alpha}$ $(\alpha = 1.25 - 1.45)$, found in the calculations, suggests that the beneficial effects of the "normal" field direction on the confinement should be more pronounced at larger ε.

1. INTRODUCTION

Over the past few years significant progress has been achieved in the experimental study of perpendicular plasma conductivity in the SOL. The main results are supplied by the Tokamak de Varennes (TdeV) [1]. This issue is important for understanding the phenomenon of the L-H transition (see refs. in [1]), development of electric biasing schemes to actively control the SOL plasma [2] and modelling the behaviour of Langmuir probes in a strong magnetic field [3,4]. Alongside phenomenological modelling of non-ambipolar radial transport [1,5,6], a number of theories have been presented which account for classical mechanisms to drive the radial current. The latter fall broadly into two main categories, according to the emphasis on one of two particular terms in the momentum balance equation (see below).

The momentum balance equation in the plasma reads:

$$md(n\mathbf{V})/dt = \mathbf{j}\times\mathbf{B} - \nabla p - \nabla\tilde{\pi} - mn\nu_x\mathbf{V} \ , \qquad (1)$$

where the terms have their usual meaning [2]. From the component of this equation in the diamagnetic direction (i.e. within the magnetic surface, but perpendicular to the magnetic field) the response of radial current density to different terms can be assessed. Models developed in

[7-10] examined the effect of the last (neutral friction) term in Eq. (1), while the pressure gradient term was analysed in [11-14].

The most adequate treatment of these drift terms in SOL modelling can be achieved in 2D codes which include all the drifts and the real magnetic geometry. Such codes (see e.g. [15,6,16]) are presently being developed/improved. Qualitative understanding of the influence of individual terms, which can be obtained from simple analytical and numerical models, is necessary both for general understanding of SOL behaviour and for code development.

In the present work the initial aim was to examine the contribution to the radial current by the pressure gradient term in Eq. (1). This has prompted the development of a simple theory of the SOL, which, however, includes the toroidicity of the magnetic geometry as an essential element.

In Section 2 we briefly review the results of the earlier theory by Rozhansky and Tendler [12,13]. Critically analysing this theory, developed in cylindrical geometry, we point out its principal omission and explain the necessity of including toroidal effects in the SOL modelling. We find, in contrast with this earlier work, that a non-zero result for the net current through the magnetic surface can only be obtained in the framework of toroidal geometry.

In Section 3 we extend a simple isothermal inviscid model of the SOL from cylindrical to toroidal geometry. Rewriting basic equations in dimensionless variables, convenient for numerical analysis, we derive an expression for the net radial current as a function of the two free parameters of our model: toroidicity $\varepsilon = r/R$ and normalised radial electric field $M_E = E_r / c_s B_{o\theta}$. The exact figures for the current are unknown at this stage, and are subsequently found from numerical calculations.

In Section 4 we define our approach to the boundary conditions for the parallel ion velocity at the target and present results of numerical calculations, from which values of plasma current (or mobility) can then be obtained.

In Section 5 we discuss results of the numerical calculations. The discussion includes physical interpretation of the solutions obtained, comparison with experiment, and a possible explanation of the phenomenon of the dependence of the power threshold for the L-H transition on the direction of the toroidal field.

In Section 6 conclusions are drawn.

2. PRESSURE GRADIENT DRIVEN CURRENTS

Radial currents must exist in the scrape-off layer since the SOL plasma is essentially confined poloidally, i.e. the poloidal flow velocity at the targets is much less than the ion sound speed, assuming shallow angles between the field line and the targets, which is the standard situation. This good confinement occurs despite the presence of a strong poloidal pressure gradient force: the plasma pressure just in front of the targets is generally small compared with the pressure in

the SOL at the stagnation point. The small plasma pressure at the targets is related to the fact that the SOL plasma is not confined in the parallel direction, but flows out at sonic speeds, approximately, and such high flow velocities correspond to large pressure drops. The pressure at the targets is particularly small when the angle between the filed lines and the targets is shallow. Therefore the poloidal pressure gradient force has to be almost exactly compensated by a $\mathbf{j_r} \times \mathbf{B}$ force. Radial currents in the SOL are thus a general feature and are not restricted to situations where an external electric radial field has been applied.

Contribution to the radial current density by the pressure gradient in its simplest form in the cylindrical geometry follows from Eq. (1):

$$j_r = \frac{1}{B}\frac{\partial p}{r\partial\theta} \ . \tag{2}$$

By integrating this equation over poloidal angle, the total current through the magnetic surface (or the part of it in case of the double-null magnetic geometry) was obtained in [12,13]:

$$I = \frac{2\pi R}{B}(p_+ - p_-) \ , \tag{3}$$

where p_+ and $p_$are plasma pressures near the two targets terminating the SOL plasma. Starting with (3) as a basic equation, the theory [12,13] incorporated effects of the poloidal **E×B** drift and anomalous viscosity, which slows down the toroidal rotation, and derived a poloidal pressure asymmetry. Toroidal flow arises due to the build-up of pressure asymmetries between the targets. This causes parallel pressure gradients and parallel plasma flow. For the ion mobility defined as

$$\mu_i = \frac{1}{en}\frac{dj_r}{dE_r} \ , \tag{4}$$

calculations yielded [12]:

$$\mu_i = K\frac{m v_i}{2eaB_\theta B_\varphi} \ , \tag{5}$$

where K is constant of the order of unity, $v_i = \sqrt{T_i/m}$ is the ion thermal velocity, m is the ion mass, a is minor radius, and B_θ and B_φ are the poloidal and toroidal components of the magnetic field.

Eq. (2), being a fundamental equation for the theory [12,13], clearly indicates the nature of the radial current analysed as being the diamagnetic drift. One may ask, therefore, how the diamagnetic drift, which is known to be divergence-free when spatial variations of the total magnetic field are ignored (as in the approximation of cylindrical geometry), can give rise to a net radial current through the magnetic surface. This questioning is strengthened by our recent

findings in [17], where we showed that the diamagnetic flux is predominantly divergence-free throughout all of the volume occupied by the plasma. This includes the magnetic presheath (m.p.s.) near the target, where the Larmor guiding centre approximation is not valid. We derived expressions for the strong local boundary flows of ions and electrons near the target per unit toroidal length. They lead to the boundary (along the "radial" direction) electric current per unit toroidal length:

$$\frac{I}{2\pi R} = \pm \frac{p}{B} \ , \tag{6}$$

where the signs of the right hand side expression are opposite for the two targets terminating the SOL plasma. It is clear from this formula, that the same boundary current can be obtained from the plasma equilibrium equation, Eq.(2), assuming sharp pressure drops down to zero near the targets. These local boundary currents at the two targets should be added to the radial current (3), thereby giving the total integrated current over the magnetic surface, including the m.p.s. and Debye sheath contributions. The total net radial current then equals zero, the result one would obtain by continuing integration of Eq. (2) through to the target surfaces, where $p \approx 0$, provided the angle between field lines and the surface is small.

Due to poloidal variations of both the magnetic field and the surface area, it can be expected that in toroidal geometry the result of the integration of the radial current density (2) over the magnetic surface (just before the entrance to the m.p.s. at both targets) should differ from (3). The total radial current through the magnetic surface, which includes the boundary flows, therefore, does not automatically have to be zero, once toroidal effects are brought into the analysis.

3. BASIC EQUATIONS

3.1 Cylindrical geometry

As a starting point we use a simple isothermal, inviscid model capable of reproducing the principal features of the SOL, which has been widely used, see for example [18]. We will later extend it to include the effects of curvature of the field lines and the radial electric field. Continuity and momentum equations lead to the two equations for the distribution of plasma density $n(s_{||})$ and parallel velocity $V_{||}(s_{||})$ along parallel coordinate $s_{||}$:

$$\frac{d}{ds_{||}}(nV_{||}) = S_p \ , \tag{7}$$

$$V_{||}\frac{dV_{||}}{ds_{||}} = -\frac{c_s^2}{n}\frac{dn}{ds_{||}} - \frac{S_p}{n}V_{||} \ . \tag{8}$$

In these equations $c_s = \sqrt{(T_i + T_e)/m}$ is the ion sound speed and S_p is the source rate of particles due to cross-field transport. The last term in Eq. (8) has appeared due to the assumption that particles supplied from the core to the SOL are with zero velocity, and their acceleration in the SOL up to the local speed $V_{||}(s_{||})$ exerts, in effect, a drag force on the plasma. By substituting S_p from Eq. (7) to Eq. (8), the latter can also be written in conservative form. For comparison with a full version of this equation in toroidal geometry (see Eq. (12)), we give here this form of the equation, allowing also for non-steady-state conditions:

$$\frac{\partial}{\partial t}(nV_{||}) + \frac{d}{ds_{||}}\left(nV_{||}^2\right) = -c_s^2 \frac{dn}{ds_{||}} \ . \tag{8a}$$

Combining Eqs. (7) and (8), and introducing Mach number $M = V_{||}/c_s$ gives:

$$\frac{dM}{ds_{||}} = \frac{S_p}{nc_s} \frac{(1+M^2)}{(1-M^2)} \ . \tag{9}$$

Two simple possibilities, considered in [18], are available for the choice of the particle source term S_p: one is S_p=Cn (C being a constant), and another, $S_p = S_0$ (constant). Little difference between the two solutions for $M(s_{||})$ is found. As we, however, are going to introduce a radial electric field into the analysis and, hence, should be expecting significant variations of the plasma density over the magnetic surface, the choice of the $S_p(n)$ dependence can become important. An intrinsic problem for the 1-D analysis of the SOL is posed by the boundary between the core plasma and the SOL: the density is poloidally uniform in the core, while large poloidal variations can occur in the SOL. We will treat the plasma according to the SOL equations, analysing plasma some distance away from the separatrix, thereby avoiding analysis of the boundary layer right near the separatrix. If for some reason (e.g. poloidal **E**×**B** drift) the density increases at a certain poloidal location, this should lead to an increase in the particle supply to the "main" SOL due to diffusion. Therefore, we will choose S_p=Cn for the particle source rate dependence on the density. Such a choice should also help us to justify a one-dimensional treatment of the SOL and the assumption that the density fall-off length λ_{sol} is poloidally constant. Thus, we adopt for the particle source rate

$$S_p = D_\perp n/\lambda_{sol}^2 \ , \tag{10}$$

and Eq. (9) becomes

$$\frac{dM}{ds_{||}} = \frac{D_\perp}{c_s \lambda_{sol}^2} \frac{(1+M^2)}{(1-M^2)} \ . \tag{11}$$

3.2 Toroidal geometry

We now write full momentum and continuity equations in curvilinear coordinates with the aim of extracting from them the effects of toroidicity and radial electric field. The final momentum balance equation should be reduced to Eq. (11) in the case of zero toroidicity, $\varepsilon = 0$, and zero radial electric field. From [15], the parallel momentum equation in curvilinear orthogonal "radial" and "poloidal" coordinates u^r and u^θ (with derivatives over the third coordinate, along the toroidal direction, ignored due to the assumption of toroidal symmetry) can be written in the form:

$$\frac{\partial}{\partial t}(\rho V_{||}) - \frac{1}{\sqrt{g}}\frac{\partial}{\partial u^\theta}\left[\frac{\sqrt{g}}{h_\theta} 2\eta_o \frac{B_\theta}{B}\left(\frac{2}{3}\frac{B_\theta}{B}\frac{1}{h_\theta}\frac{\partial V_{||}}{\partial u^\theta} - \frac{1}{3}\frac{B_\varphi}{B}\frac{1}{h_\theta}\frac{\partial V_\perp}{\partial u^\theta} - \frac{1}{3}\frac{1}{h_r}\frac{\partial V_r}{\partial u^r}\right)\right] + \frac{1}{\sqrt{g}}\left[\frac{\partial}{\partial u^\theta}\left(\frac{\sqrt{g}}{h_\theta}\rho V_\theta V_{||}\right) + \frac{\partial}{\partial u^r}\left(\frac{\sqrt{g}}{h_r}\rho V_r V_{||}\right)\right] + \rho V_\perp V_\varphi \frac{\partial \ln h_\varphi}{h_\theta \partial u^\theta} = S_{mv_{||}} - \frac{B_\theta}{B}\frac{1}{h_\theta}\frac{\partial p}{\partial u^\theta} \quad . \tag{12}$$

Here $\rho = mn$ is mass density, η_o is classical ion parallel viscosity, $S_{mv_{||}}$ is the parallel momentum source term due to interaction with neutrals etc.; h_r, h_θ and $\sqrt{g}$ are metrics indexes (see [15] for definitions, also Eqs. (16,17)). Perpendicular velocity $V_\perp$ is the velocity in the diamagnetic direction, i.e. within the magnetic surface, but perpendicular to the magnetic field.

Eq. (12) includes the most important terms of the parallel momentum equation that can be found in Eq. (2.93) of ref. [15]. An important term with $V_\perp V_\varphi$ on the left hand side (l.h.s.) of this equation is concealed inside the term $\chi_{div,||}$ of the Eq. (2.93). Often, anomalous viscosity terms $-\frac{1}{\sqrt{g}}\left[\frac{\partial}{\partial u^\theta}\left(\frac{\sqrt{g}}{h_\theta^2}\eta_\theta\frac{\partial V_{||}}{\partial u^\theta}\right) + \frac{\partial}{\partial u^r}\left(\frac{\sqrt{g}}{h_r^2}\eta_r\frac{\partial V_{||}}{\partial u^r}\right)\right]$ are added to the l.h.s. of the momentum equation (12) (see e.g. Eq. (3.7) of [15]).

As we are considering the simplest case of a stationary inviscid plasma with no neutral sources and other damping mechanisms, we can neglect the first two terms on the l.h.s. and the first term on the r.h.s. of Eq. (12). It is conceivable, however, that viscous forces could become the dominant ones in certain conditions, in particular near the separatrix layer, where a strong shear in parallel plasma flow is expected. Here, as we indicated in the previous section, we model plasma some distance away from the separatrix, extending the simple model described in [18]. Thus we neglect viscous terms. Further, as we intend to use a 1-D SOL model and are not interested in the "fine" radial structure of the scrape-off layer, we can also neglect the term with $\partial/\partial u^r$ on the l.h.s. The integral of this term across the SOL width is almost zero, since $V_{||} = 0$ at the last closed flux surface (LCFS), $\rho = 0$ at the wall, and $\sqrt{g} \approx const$ across the SOL due to its small thickness compared to the minor radius. So, we end up with the following equation for the momentum balance:

$$\frac{1}{\sqrt{g}}\frac{\partial}{\partial u^{\theta}}\left(\frac{\sqrt{g}}{h_{\theta}}\rho V_{\theta}V_{\|}\right)+\rho V_{\perp}V_{\varphi}\frac{\partial ln\, h_{\varphi}}{h_{\theta}\partial u^{\theta}}=-\frac{B_{\theta}}{B}\frac{1}{h_{\theta}}\frac{\partial p}{\partial u^{\theta}}\ . \tag{13}$$

The continuity equation from [15] reads:

$$\frac{\partial}{\partial t}(n)+\frac{1}{\sqrt{g}}\frac{\partial}{\partial u^{\theta}}\left(\frac{\sqrt{g}}{h_{\theta}}nV_{\theta}\right)+\frac{1}{\sqrt{g}}\frac{\partial}{\partial u^{r}}\left(\frac{\sqrt{g}}{h_{r}}nV_{r}\right)=S_{n}\ , \tag{14}$$

where S_n is the particle source term due to ionisation. For the steady state conditions with no ionisation Eq. (14) is reduced to

$$\frac{1}{\sqrt{g}}\frac{\partial}{\partial u^{\theta}}\left(\frac{\sqrt{g}}{h_{\theta}}nV_{\theta}\right)+\frac{1}{\sqrt{g}}\frac{\partial}{\partial u^{r}}\left(\frac{\sqrt{g}}{h_{r}}nV_{r}\right)=0\ . \tag{15}$$

Since in our simple model we will not analyse radial fluxes due to radial **E×B** drift, the second term in this equation includes only radial diffusion, while the first term should include the poloidal flux caused by both parallel velocity and poloidal **E×B** drift.

To progress further from Eqs. (13) and (15), we need to specify the magnetic geometry. We opt for the simplest geometry bearing features of the single null X-point divertor magnetic configuration with low X-point height. The geometry is shown on Fig.1, and is the one with poloidally constant scrape-off layer width equal to λ_{sol} and magnetic surfaces being concentric circles in the poloidal cross-section. This gives $B_{\varphi} \sim 1/R$, $B_{\theta} \sim 1/R$ for toroidal and poloidal components of the magnetic field, and for the value of the safety factor: $q=\frac{r}{R_o}\frac{B_{\varphi}}{B_{\theta}}=const\,(\theta)$. The direction of the increase in toroidal angle φ is assumed to be against the main plasma current (the direction of plasma current itself does not affect the problem in any way). Positive particle velocity (i.e. particle moving along a field line in the direction of increasing φ) should also imply positive poloidal velocity, i.e. motion from the inner to the outer target (increasing θ).

From the expression for the element of length ds in our orthogonal geometry:

$$(ds)^2=(dr)^2+(rd\theta)^2+(Rd\varphi)^2\ , \tag{16}$$

we can derive metrics indexes:

$$
\begin{aligned}
h_\theta &\equiv \frac{ds}{d\theta} = r \\
h_\varphi &\equiv \frac{ds}{d\varphi} = R \\
h_r &\equiv \frac{ds}{dr} = 1 \\
\sqrt{g} &\equiv h_\theta h_\varphi h_r = rR
\end{aligned}
\tag{17}
$$

Substituting these coefficients in Eqs. (13) and (15), and replacing u^r and u^θ by r and θ, we obtain:

$$
\begin{cases}
\dfrac{B_\theta}{B}\dfrac{\partial}{\partial\theta}(p) + \dfrac{1}{R}\dfrac{\partial}{\partial\theta}(RnmV_\theta V_{||}) + nmV_\perp V_\varphi \dfrac{1}{R}\dfrac{\partial R}{\partial\theta} = 0 \\
\dfrac{\partial}{\partial\theta}(RnV_\theta) - aRn\dfrac{D_\perp}{\lambda_{sol}^2} = 0
\end{cases}
\tag{18}
$$

In the continuity equation (second in (18)) we neglected variations of minor radius across the SOL compared with density decay in the $\partial/\partial r$ term, and replaced V_r by $D_\perp/\lambda_{sol}$.

One important consequence of replacing cylindrical with toroidal geometry can easily be demonstrated. Introducing parallel coordinate $s_{||}$ into the momentum equation in (18) by the substitution $\dfrac{\partial}{\partial\theta} \to r\dfrac{B}{B_\theta}\dfrac{\partial}{\partial s_{||}}$, and considering the case of zero radial electric field (so that $V_\theta = V_{||}\cdot B_\theta/B$, $V_\perp = 0$), one can derive:

$$
\frac{\partial}{\partial s_{||}}(nmV_{||}^2 + p) + nmV_{||}^2\frac{1}{R}\frac{\partial R}{\partial s_{||}} = 0 \ . \tag{19}
$$

So, in toroidal geometry the parallel stress $(nmV_{||}^2 + p)$ is no longer constant along the field line, unlike the situation in cylindrical geometry. For this reason, plasma pressures at the inner and outer targets do not necessarily have to be equal even when parallel velocities are.

Equations (18) for the case of zero electric field can, alternatively, be obtained from the standard gas dynamic expressions for 1-D flow in a duct of variable cross-section area A [19]:

$$
\frac{d}{ds_{||}}(nV_{||}A) = S_n A \tag{20}
$$

for particle conservation, and

$$
\frac{d}{ds_{||}}(nmV_{||}^2 A) = -A\frac{dp}{ds_{||}} \tag{21}
$$

for momentum conservation; also $A \cdot B = const$. Influence of the poloidal variation of the cross-section A and the position of the limiter on the SOL width has been analysed in [20].

We now introduce the effect of radial electric field on the poloidal and perpendicular velocities. Neglecting the small difference between projections of a vector on poloidal and perpendicular directions, we can write:

$$\begin{cases} V_\perp = \dfrac{R}{R_o} V_o \\ V_\theta = \Theta V_{||} + \dfrac{R}{R_o} V_o \end{cases}, \tag{22}$$

where $\Theta \equiv B_\theta / B$, $V_o \equiv E_r / B_o$, B_o being the magnetic field on the magnetic axis, at r=0. Also, by introducing $M = V_{||}/c_s$, $M_E = V_o / \Theta c_s$ (thus $M_E = 2\gamma$, where γ was the symbol used in [21,22]), $\xi = R/R_o = 1 + \varepsilon \sin\theta$, $q = \dfrac{a}{R_o}\dfrac{1}{\Theta}$ and

$$F = \frac{qR_o D_\perp}{\lambda_{sol}^2 c_s}, \tag{23}$$

the momentum and continuity equations can finally be written in dimensionless form (one can normalise density by any value, as it enters both equations linearly):

$$\begin{cases} \dfrac{\partial}{\partial\theta}(n) + \dfrac{1}{\xi}\dfrac{\partial}{\partial\theta}\left[\xi n M (M + \xi M_E)\right] + n M M_E \dfrac{\partial\xi}{\partial\theta} = 0 \\ \dfrac{\partial}{\partial\theta}\left[\xi n (M + \xi M_E)\right] - F n \xi = 0 \end{cases}, \tag{24}$$

where we replaced pressure by nmc_s^2 in the momentum balance equation (first in (18)), and neglected the small difference between V_φ and $V_{||}$. These equations can be solved for the derivatives of the Mach number and the density:

$$\begin{cases} M' = \dfrac{F[1 + M(M + \xi M_E)] - M\dfrac{\xi'}{\xi}(1 - \xi M M_E - \xi^2 M_E^2) - 2\xi' M_E}{1 - (M + \xi M_E)^2} \\ \dfrac{n'}{n} = -MF - M'(M + \xi M_E) - M M_E \xi' \end{cases}, \tag{25}$$

where $M' \equiv \partial M/\partial\theta$, $n' \equiv \partial n/\partial\theta$, $\xi' \equiv \partial\xi/\partial\theta = \varepsilon \cos\theta$. Thus a numerical solution is readily obtained (see below).

The two free parameters in these equations are the toroidicity $\varepsilon = a/R_o$, which is present in the expression for ξ, and "electric" Mach number M_E. $|M_E| = 1$ means that poloidal

rotation due to the poloidal **E×B** drift at $\theta = 0$ is equal to the poloidal rotation of a particle moving with the ion sound speed.

For the simplest case of no toroidicity ($\varepsilon = 0$), and zero electric field ($M_E = 0$), Eqs. (24) lead to:

$$\frac{\partial M}{\partial \theta} = F\frac{1+M^2}{1-M^2} \ , \tag{26}$$

which is essentially the same as Eq. (11). F is the usual eigenvalue, of order unity, whose precise value is such as to make the source fit the space available. For $F \approx 1$ and $qR_o \approx L$, the connection length, one obtains from Eq. (23) the familiar expression relating $D_\perp$ and λ_{sol}, namely, $\lambda_{sol} \approx \left(LD_\perp / c_s\right)^{1/2}$.

3.3 Net radial current and mobility

Similar to the parallel momentum and continuity equations (12,13), which were used to write equations for plasma density and parallel velocity, one can use the momentum equation in the diamagnetic direction (i.e. within the magnetic surface but perpendicular to the field line) to find the radial particle flux. From Eq. (2.103) of ref. [15], by ignoring negligible terms, one can obtain:

$$\begin{aligned}
&\frac{\partial}{\partial t}(\rho V_\perp) + \frac{1}{\sqrt{g}}\left[\frac{\partial}{\partial u^\theta}\left(\frac{\sqrt{g}}{h_\theta}\rho V_\theta V_\perp\right) + \frac{\partial}{\partial u^r}\left(\frac{\sqrt{g}}{h_r}\rho V_r V_\perp\right)\right] + \\
&\frac{1}{\sqrt{g}}\frac{\partial}{\partial u^\theta}\left[\frac{\sqrt{g}}{h_\theta^2}\eta_o\left(\frac{2}{3}\frac{B_\theta B_\varphi}{B^2}\frac{\partial V_{||}}{\partial u^\theta} - \frac{1}{3}\frac{B_\varphi^2}{B^2}\frac{\partial V_\perp}{\partial u^\theta}\right)\right] = \\
&-\frac{B_\varphi}{B}\frac{1}{h_\theta}\frac{\partial p}{\partial u^\theta} + \rho V_\varphi V_{||}\frac{\partial \ln h_\varphi}{h_\theta \partial u^\theta} + j_r B + S_{mv_\perp} \ .
\end{aligned} \tag{27}$$

The term with $V_\varphi V_{||}$ on the r.h.s. of this equation is concealed inside the term $\chi_{div,\perp}$ of the Eq. (2.103) of [15]. Keeping only main terms while neglecting viscous, external momentum source (which can be large, but we are not discussing it in the present paper) and other smaller terms, one obtains for the radial current density:

$$j_r = \frac{B_\varphi}{B^2}\frac{1}{h_\theta}\frac{\partial p}{\partial u^\theta} - nmV_\varphi V_{||}\frac{1}{B}\frac{1}{h_\theta}\frac{\partial \ln h_\varphi}{\partial u^\theta} \ . \tag{28}$$

Using metrics indexes for our simple geometry (17) and neglecting the small difference between V_φ and $V_{||}$, B_φ and B, leads to:

$$j_r = \frac{1}{B}\frac{\partial p}{r\partial\theta} - \frac{nmV_{\|}^2}{RB}\cos\theta \ . \tag{29}$$

The second term on the r.h.s. describes the effect of the centrifugal drift which only appears in toroidal geometry.

Eq. (29) can also be written in the form:

$$j_r = \frac{e\rho_s c_s}{r}\left(\xi\frac{\partial n}{\partial\theta} - \varepsilon n M^2 \cos\theta\right), \tag{30}$$

where $\rho_s = c_s/\omega_{io}$ and $\omega_{io} = eB_o/m$. By integrating this equation over the magnetic surface (including the surface area factor $\sim\xi$) from the entrance to the inner target m.p.s. to the entrance to the outer target m.p.s., and adding contributions from each m.p.s. layer (6), we obtain:

$$\frac{I_r}{2\pi R_o} = e\rho_s c_s\left[\int_{-\pi}^{+\pi}\left(\xi^2\frac{\partial n}{\partial\theta} - \xi\varepsilon n M^2\cos\theta\right)d\theta + \left(n_{in} - n_{out}\right)\right]. \tag{31}$$

Here $n_{in} = n(-\pi)$ and $n_{out} = n(+\pi)$, and I_r is the total current across the magnetic surface.

It has to be noted that the magnitude of the radial current density j_r strongly depends on the poloidal position, and the continuity of the current flow, $div\mathbf{j} = 0$, gives rise to parallel currents within the SOL. These parallel currents are effectively Pfirsch-Schlüter currents. The effect of these currents on the SOL and divertor behaviour has previously been analysed in [11]. However, in this paper centrifugal drift was ignored. A correct treatment of the Pfirsch-Schlüter currents in the SOL and divertor regions and their effect on the MHD equilibrium has recently been given in [14].

It is convenient, for the purpose of future numerical calculations, to introduce the normalised net radial current per unit toroidal length:

$$I^* = \frac{I_r}{2\pi R_o}\Big/ e\langle n\rangle\rho_s c_s, \tag{32}$$

where the surface averaged density is defined as

$$\langle n\rangle = \frac{1}{2\pi}\int_{-\pi}^{+\pi}\xi n\cdot d\theta \ . \tag{33}$$

With the dependence of I^* on M_E supplied from numerical calculations, it will be easy to derive a dimensional expression for plasma mobility μ:

$$\mu = \frac{mc_s}{2\pi e a B_\theta B_\varphi} \frac{dI^*}{dM_E} , \tag{34}$$

where we defined μ in a differential way as

$$\mu = \frac{1}{e\langle n \rangle} \frac{d\langle j_r \rangle}{dE_r} , \tag{35}$$

and $\langle j_r \rangle$ was assumed to be the surface averaged net radial current density:

$$\langle j_r \rangle = \frac{I_r}{4\pi^2 a R_o} . \tag{36}$$

Obvious similarities between (34) and (5) with respect to dependencies on temperature, minor radius, toroidal and poloidal fields, can be seen. However, it is clear from (31) that with neglect of toroidicity ($\varepsilon = 0$) net radial current must be equal to zero, and Eq. (5) can not be justified.

4. NUMERICAL RESULTS

4.1 Boundary conditions

Equations (25) were solved numerically for different ε and M_E, and poloidal distributions of Mach number and density were used to calculate normalised current I^* according to (31,32). The continuity equation (second in (24)) has free parameter, or eigenvalue, F defined by (23). This parameter has to be found from calculations by satisfying boundary conditions on the Mach number for the parallel particle flow at the two targets. Since the Mach number at one target can be set explicitly (calculations start at a particular target, where boundary conditions have been pre-set), F is found from the requirement that boundary conditions are fulfilled at the other target.

The boundary conditions we adopted for the present calculations are the so called "intuitive" boundary conditions in the presence of a poloidal **E×B** drift [21]. They prescribe that the total poloidal ion velocity at the entrance to the magnetic pre-sheath (m.p.s.), when ignoring the diamagnetic drifts contribution, is at least $c_s \cdot B_\theta / B$. Therefore, for the minimum (absolute magnitude) value of the Mach number near a target we have:

$$\begin{cases} M|_{\theta=-\pi} = -1 - M_E \\ M|_{\theta=+\pi} = +1 - M_E \end{cases} . \tag{37}$$

For the "natural" (unbiased) radial electric field in the SOL,

$$E_r = -\frac{\Psi}{e}\frac{dT_e}{dr} \ , \tag{38}$$

where Ψ is usually ≈ 3, and radial decay of electron temperature is assumed, the effect of boundary conditions (37) would be to increase the absolute value of the Mach number at the inner target and to reduce it at the outer target.

The strategy we adopted in finding the numerical solutions of equations (25) was to keep boundary conditions fixed as prescribed by (37), until a smooth $M(\theta)$ solution was lost. Often solutions oscillated approaching the inner target. This could occur at non-zero ε, especially when the effect of radial electric field was to push particles towards the inner target, so that the imposition of the strict conditions (37) implied a forced reduction of the Mach number at the target. The sonic transition, achieved when the denominator in the first of the equations (25) was zero:

$$M + \xi M_E = \pm 1 \ , \tag{39}$$

was then reached inside the plasma some distance away from the target, i.e. a "free-standing" sonic transition. Thus, solutions satisfying (37) could still be obtained, but $M(\theta)$ oscillated over a certain range of poloidal angles. In order to avoid oscillations, we relaxed boundary conditions (37) at the inner target when such problems occurred. We had to raise the coefficient F until a smooth transition through the sonic transition (39) was obtained. The absolute value of the Mach number at the inner target then, of course, was larger than prescribed by (37), which only specifies minimum values.

4.2 Solutions of the equations

We will first illustrate some particular solutions of Eqs. (25) and then give the summary of results. Fig. 2 shows solutions for the Mach number and the density for the simplest case of $\varepsilon = 0$ and $M_E = 0$, i.e. cylindrical approximation with no radial electric field. The solution for the Mach number can also be obtained from (29) in analytical form [18]. On this and following figures the density profile $n(\theta)$ was normalised to the density at the inner target, $n_{in} \equiv n(-\pi)$.

Fig. 3, representing $\varepsilon = 0.33$, $M_E = 0$ case, shows the effect of toroidicity by itself. The ratio of densities between outer and inner targets is n_{out}/n_{in}=1.23, indicating the appearance of pressure imbalance in favour of the outer target. The normalised radial current $I^* = -0.224$, its negative value implying the inward direction.

The radial electric field in the simplest case of no toroidicity, $\varepsilon = 0$, acts in a straightforward way by creating density asymmetries in favour of the target to which the particles are scooped by the poloidal **E×B** drift. This effect was first analysed in [23]. For $M_E = -0.4$, which implies "unnatural" (negatively biased), radial electric field, the results are shown in Fig. 4. Substantial density asymmetry has developed in favour of the inner target with

n_{out}/n_{in}=0.671. The radial current, as expected for a cylindrical case, is zero. As can be seen in Fig. 4, boundary conditions were fixed according to (37), and so the Mach number is equal to -0.6 at the inner target and +1.4 - at the outer target.

Fig. 5 presents the results of the $\varepsilon = 0.33$, M_E=-0.4 case. Strict boundary conditions (37) had to be relaxed at the inner target in order to avoid earlier onset of the sonic transition (39) (before the target was reached), manifested by appearance of oscillations in the solution for $M(\theta)$. Thus, instead of M=-0.6, which would be in accordance with boundary conditions (37), the Mach number at the inner target had to be reduced to M=-0.883. Due to additional plasma acceleration at the inner target from M=-0.6 to M=-0.883, the density ratio n_{out}/n_{in}, instead of being significantly lower than in the case without electric field shown on Fig. 3 (n_{out}/n_{in}=1.224), is only marginally smaller than that: n_{out}/n_{in}=1.195. Normalised current for this case is I^*=-0.31.

Fig. 6 shows the result of increasing toroidicity up to $\varepsilon = 0.5$ in the absence of radial electric field. In this case of high toroidicity, no solutions satisfying boundary conditions (37) could be obtained. The point on the $M(\theta)$ profile where the effective sound barrier was overcome, is indicated by the arrow. Mach number at the inner target reaches -1.50, and the density falls substantially, resulting in n_{out}/n_{in}=2.50. Normalised current for this case is I^*=-0.448.

The results of the calculations of the Mach number at the inner target at different ε and M_E are summarised in Fig. 7. No computational problems related to the onset of the free-standing sonic transition (39) were observed near the outer target, and the Mach number at this target always satisfied the boundary conditions (37). As can be seen from Fig. 7, boundary conditions (37) could also be fulfilled at the inner side for $\varepsilon = 0$. For non-zero ε, however, there were regions of M_E, where smooth solutions satisfying (37) could not be obtained, and the effective sound barrier was achieved inside the plasma, with further parallel plasma acceleration towards the inner target. Ultimately, at $\varepsilon = 0.5$ and $\varepsilon = 0.75$, for all M_E values Mach number at the inner target was above the one prescribed by (37).

Fig. 8 summarises results for the density ratio n_{out}/n_{in}. They are closely related to the results for the Mach number discussed above. Monotonic rise of n_{out}/n_{in} versus M_E is seen for $\varepsilon = 0$ (results are the same as in Fig.4 [22]), while for non-zero ε a density fall near the inner target due to plasma acceleration above the effective sound barrier (39) is observed. n_{out}/n_{in} ratios not plotted on Fig.4 are equal to 13.5, 17.4, 22.2 for $\varepsilon = 0.75$ and M_E=0.6, 0.8, 1.0 respectively.

Fig. 9 shows variations of eigenvalue F, defined by (23), for different cases of ε and M_E. Relatively small variations of F between ≈0.12 and ≈0.2 for most of the cases, except for $\varepsilon = 0.5$ and $\varepsilon = 0.75$ and extreme values of M_E, imply that for a given plasma temperature, safety factor and major radius, the coefficient relating λ_{sol} with $\sqrt{D_\perp}$ is fairly constant, within a factor of 1.29.

Finally, the results of calculating the normalised current I^* are presented in Fig. 10. The current was always negative, i.e. inward. Its dependence on the radial electric field is weak an inconsistent with the assumption of constant plasma mobility μ. There is an indication of regions of negative mobility at positive M_E for $\varepsilon = 0.2$ and 0.33, and at negative M_E for $\varepsilon = 0.75$. As a function of the toroidicity, for M_E around zero, the dependence $I^* \sim \varepsilon^{\alpha}$ with $\alpha = 1.25 - 1.45$ is observed. The results will be discussed in Section 5.1.

For cases where large n_{out}/n_{in} ratio was calculated, the results could have been affected by imperfections of our 1D model. In particular, by the choice of the particle source term: $S_p = Cn$, as discussed in Section 3.1. For large variations of density along the magnetic surface, significant perpendicular flows of particles through the separatrix should be expected, which could affect particle supply to the "main" SOL. This effect has not been taken into account in our model.

5. DISCUSSION

5.1 Physical interpretation of the origin of the radial current

The origin of the pressure gradient driven current can be understood from Fig. 11. Due to the pressure drop towards the target, the direction of the diamagnetic current is inwards on the outboard side and outwards - on the inboard side of the SOL. The inverse dependence of the diamagnetic current on the magnitude of the toroidal field (see Eq. (29)) together with larger area of the outboard side of the magnetic surface compared to the inboard one, should result in net inward current. For the opposite direction of the magnetic field the current should be outward (see Section 5.4). The above interpretation has the same basis as was used in the papers [24,25] which analysed neoclassical ion heat transport through the separatrix. Some details of these models will be touched upon in Section 5.7.

Following the above interpretation, we can easily derive a crude estimate of the radial current. By assuming up-down pressure asymmetry of the order of the pressure itself, $\Delta p \sim p$, the total particle flow per unit toroidal length through inboard and outboard sides can be estimated as $\pm p/B$, where the sign is plus for the inboard side and minus - for the outboard one. The relative difference in the magnitude of the toroidal field between the two sides, $\sim \varepsilon$, gives for the poloidal average the value of $\approx \varepsilon p/B$. For the surface averaged radial current density one can obtain:

$$| j_r | \approx enc_s \varepsilon \frac{\rho_s}{2\pi a} \ . \tag{40}$$

The above estimate ignores shifts in the maximum of the poloidal pressure distribution away from $\theta = 0$ due to both toroidal effects (see an example of such a shift in Fig. 3) and the

radial electric field. It also neglects the contribution of the centrifugal drift (Eq.(29)) which tends to diminish the magnitude of the net radial current. Nevertheless, it turns out to be fairly accurate. From Fig. 10, for the case of $\varepsilon = 0.33$, around M_E=0, the normalised radial current is equal to $I^* = -0.22$. Remembering the definition of the normalised current given by (30), the surface averaged current density can be obtained as

$$| j_r | = 0.22 enc_s \frac{\rho_s}{2\pi a} = 0.22 \frac{p}{2\pi a B} , \qquad (41)$$

which is close to (40) in magnitude. As a function of ε, the net current obtained from the numerical calculations around M_E=0, scales as $j_r \sim \varepsilon^{\alpha}$ with $\alpha = 1.25 - 1.45$ (see Section 4.2). For $\varepsilon = 0$, the current j_r is equal to zero, it may be emphasised again.

Changes to the total particle flow and potential profile introduced by the pressure gradient driven current should, ideally, be included in a more detailed SOL model in a self-consistent way. This goes beyond the scope of the present paper. Here we will only demonstrate that the nature of the current discussed ensures self-consistency in one extreme case, which is unlikely to happen in a real experiment. Let us consider an insulating target, so that no charge sink to the target is allowed and, therefore, net radial current has to be constant along the minor radius. Due to the radial density decay in the SOL, the current near the wall should be zero. Thus, it has to be zero everywhere in the SOL. This situation seems to contradict the fact that the net radial current, according to Fig. 10, is a fairly constant function of M_E, implying the unlimited growth of the radial electric field in the SOL due to the passage of the pressure gradient driven current. Some indication of the decay of the current at high M_E can, however, already be seen in Fig. 10. We have performed calculations for high M_E values, in the range of +1 to +2, for a particular case of $\varepsilon = 0.33$, in order to assess whether the current can be brought down to zero at very high M_E. The results of these calculations are presented on Fig. 12. As M_E is increased above +1, the current continues to increase and reaches I^*=+0.126 at M_E=+2. The reversal of the sign of the current can be attributed to the effect of large centrifugal drift (proportional to M_E) in the vicinity of the inner target, with the Mach number for the parallel ion velocity reaching -4.2 at this target. These results ensure that even in our idealistic case of insulating targets and the pressure gradient driven current being the only source of radial current (no anomalous contributions, currents due to the interaction with neutrals etc.), the problem has a self-consistent solution. For the more realistic case of conducting targets, the radial currents will close within the SOL by parallel currents to the target.

5.2 Radial particle flow

It may appear from Eqs. (29) and (31) that both ions and electrons contribute to the net radial current. This is because expressions for the current include total pressure. It can be demonstrated, however, that the ambipolar flow caused by the radial **E**×**B** drift should

compensate the fraction of the radial current carried by electrons. This conclusion is not a universal one, but it should apply to the conditions for which our model is an approximation: isothermal plasmas with no friction between electrons and ions. In these conditions electrons are distributed according to the Boltzmann law:

$$n = n_o exp\left(\frac{e\Phi}{T_e}\right) . \tag{42}$$

Neglecting the small difference between B_φ and B, we can write for the radial electron flux:

$$\Gamma_e^r = -\frac{1}{eB}\frac{\partial p_e}{r\partial\theta} - n\frac{E_\theta}{B} , \tag{43}$$

which can be transformed into:

$$\Gamma_e^r = -\frac{n}{rB}\left(\frac{T_e}{e}\frac{\partial ln\, n}{\partial\theta} - \frac{\partial\Phi}{\partial\theta}\right) . \tag{44}$$

It is clear from this equation that substituting the density from (42) gives zero Γ_e^r. Therefore, the electron radial flux should be equal to zero even locally, at each poloidal angle. This conclusion holds over all the magnetic surface including the magnetic pre-sheath (m.p.s.) and Debye sheath, provided no strong electron parallel current, comparable to the electron saturation current, flows onto the target.

In our model we do not directly calculate flow caused by the radial **E×B** drift. Whereas strong local **E×B** radial flows in the m.p.s. and Debye sheath can be analytically included (see results of [17]), calculation of the radial fluxes distributed over the magnetic surface due to the presence of the poloidal electric field is outside the scope of our model, since we did not include the radial **E×B** drift in the continuity and momentum equations. Such a neglect of the radial **E×B** drift over the poloidal **E×B** drift is justified when the divergence of the poloidal flux, $\frac{\partial}{r\partial\theta}\left(n\frac{E_r}{B}\right)$, significantly exceeds the divergence of the radial flux, $\frac{\partial}{\partial r}\left(n\frac{E_\theta}{B}\right)$. It can be shown that this condition is equivalent to $\Psi >> 1$, where Ψ (Eq. (38)) is usually ≈ 3. This matter is discussed further in [22].

Since electrons do not carry any radial current, the net radial current through the magnetic surface should be fully attributable to ions, and the plasma mobility μ that we defined in (33) is in effect ion mobility μ_i. Thus the radial current consists of two ion currents, one part due to diamagnetic and centrifugal drift, and another - due to radial **E×B** drift. This sum is also equal to the value calculated in this paper, i.e. due to ion and electron diamagnetic currents plus the ion centrifugal drift.

5.3 Origin of the free-standing sonic transition near the inner target

The sound barrier (sonic transition) is often reached before a target in numerical codes for the scrape-off layer. The simplest cause of such free-standing sonic transition is a variation of temperature (falling) in approaching the target which is more rapid than the variation in parallel particle flux density (increasing) [26,27]. Other factors such as area change of the flux tube can also play a role [28]. As can be seen from Fig. 7, the free-standing sonic transition tends to occur at high toroidicities, and is usually facilitated by large negative electric fields.

The effect of toroidicity could be qualitatively explained by the analogy with the behaviour of a gas in a nozzle. It was observed in numerical calculations that the sonic transition occurs approximately at $\theta \approx -1.8 - 1.9$ rad, i.e. shortly after the ion flow, moving towards the inner target, passes the midplane position at $\theta = -\pi/2 \approx -1.57$ rad. On its way to the inner target, the ion flow is being compressed in the region of θ between 0 and $-\pi/2$ due to the toroidal effect of the reduction in the area of perpendicular cross-section of the ion flow. This effect, which is absent in a cylindrical geometry, does not act on its own, but facilitates "natural" acceleration of the ion flow due to the sink of ions to the target. Further downstream, after the sound barrier is overcome, there is an expansion of the perpendicular cross-section for θ between $-\pi/2$ and $-\pi$. It causes an additional acceleration of the ion flow and/or drop in plasma density. This effect has previously been discussed in [28], and is well demonstrated by the increase in the ratio n_{out}/n_{in} with the increase of toroidicity. From this explanation, it becomes clear why the free-standing sonic transition never occurred near the outer target. For the ion flow moving towards the outer target, the phases of expansion (θ between 0 and $+\pi/2$) and contraction (θ between $+\pi/2$ and $+\pi$) of the perpendicular cross-section are in the opposite sequence compared to the inboard side of the torus.

The effect of the radial electric field on the earlier onset of the sonic transition (easier for negative M_E) is relatively straightforward and follows from the condition (39). Negative M_E implies that the sonic transition can be reached at smaller absolute values of the Mach number, which makes it easier to occur.

5.4 The effect of the B_T reversal on the numerical results

Despite the fact that equations (24) were derived for the magnetic configuration shown in Fig.1, i.e. for the ion ∇B drift direction towards the target, they do not have to be changed for the opposite, or "reversed", toroidal field direction, when the ion ∇B drift is directed away from the target. The only adjustment to be made is the change of a sign of the normalised electric field, M_E. Thus, all the solutions for $M(\theta)$ and $n(\theta)$, are valid for the reversed B_T configuration, if we simply replace solutions for positive M_E by the ones for negative M_E, and vice versa.

This, however, reveals one of the deficiencies of the present model which ignores the effect of the diamagnetic drift on the main conservation equations. The non-divergence-free part of the diamagnetic drift, originating from spatial variations of the magnetic field, should contribute to both momentum and continuity equations, and its contribution will be different for opposite B_T directions. We have not included diamagnetic drift in the analysis for technical reasons: our model is one dimensional, while the proper inclusion of the diamagnetic drift requires a consideration of its both poloidal and radial components. Due to the fact that the non-divergence-free part of the diamagnetic drift mainly accounts for the vertical ∇B drift (see, e.g. [17]), it is easy to predict, on the basis of qualitative arguments presented in Section 5.1, its effect on the up-down pressure asymmetry and the net radial current. For "normal" field direction the up-down pressure asymmetry and the absolute value of the net radial current will be reduced, while for the "reversed" field both the up-down pressure asymmetry and the (outward) net radial current will be increased. This should not affect a "differential" response of the radial current to the externally applied radial electric field. Moreover, for the assumptions made about the SOL parameters in the present paper, namely, $T_e = T_i$ and $\Psi \approx 3$ (see Eq.(38)), the effect of the radial electric field on the poloidal pressure distribution is stronger, by a factor of Ψ, than the effect of the ion diamagnetic drift.

In the calculations of the radial current (30,31), the effect of the diamagnetic drift was properly included. As the two terms in the current (28,29) describe the diamagnetic and centrifugal drifts, their sign should change with the B_T reversal. Therefore, in order to transfer all the results obtained for the current (Fig. 10) on the reversed B_T case, one has to change both the sign of M_E and the sign of the current I^*. Thus, net radial current in the SOL should be outward for the reversed toroidal field.

5.5 Comparison with experiment

Direct comparison between our results on the ratio of densities between the two targets n_{out}/n_{in} and experimental data can scarcely be made, since our model does not include many features present in real experiments: temperature asymmetries between the targets due to poloidal asymmetries of the heat flux and radiation power, interaction with the neutrals etc. It is also difficult to make such a comparison on the effect of toroidal field reversal. Our model does not include any radial **E×B** drift due to a temperature drop towards the target, which generates opposite asymmetries compared to the effect of the poloidal **E×B** drift [29], and is expected to dominate over the poloidal **E×B** drift effects in high recycling regimes [22]. Survey of the results from different machines [30] shows that the ratio n_{out}/n_{in} more often increases when the toroidal field is reversed, contrary to the expected effect of the poloidal **E×B** drift. This conclusion was recently confirmed on JET [31] and Alcator C-Mod [32].

In light of these problems of comparing the density ratio n_{out}/n_{in} between our results and experiment, it seems that the most useful application of our results should be in the area of

biasing experiments. It is clear from the results of the Section 4.2, that our calculations do not lead to a constant magnitude of the ion mobility, as they indicate that the $I^*(M_E)$ dependence is rather flat. As it can be easily demonstrated, the variation of absolute values of the current I^* is also insufficient to explain the experimental data. On average, for strong negative biasing in the case of "normal" toroidal field, or strong positive biasing in the case of the "reversed" toroidal field, we can take variation of I^* over the range of M_E between -1 and 0 (see Fig. 10) as representative for the order of magnitude of dI^*/dM_E. For the case of $\varepsilon = 0.33$ we will then obtain: $dI^*/dM_E \approx 0.34$. To explain the experimentally found dependence of mobility on the main plasma current, it was found in [1] that the constant K in Eq. (5) had to be adjusted to 2.2. Taking this into account, and comparing our equation for the ion mobility Eq. (34) with Eq. (5) for $dI^*/dM_E \approx 0.34$, and assuming $c_s/v_i = \sqrt{2}$ (i.e. $T_e = T_i$), one can obtain that the correct evaluation of the ion mobility is short by a factor of about 13 to explain the experiment. This then would appear to definitely exclude the pressure gradient current as a possible candidate to explain the mobilities observed in the experiments on TdeV [1].

Another classical mechanism mentioned in [1] as a candidate to partly explain the TdeV data, is radial current which comes from the friction force exerted on the induced toroidal and poloidal flow due to ion-neutral collisions. The ion mobility, quoted in [1], can be deduced from the expression for the local radial current density inside the plasma given in [10] (Eq. (7) of this ref.):

$$\mu_i = \frac{m_i n_n \langle \sigma v \rangle_{CX}}{e B_\theta^2} \quad . \tag{45}$$

Here n_n is the neutral density. This "local" ion mobility, however, ignores contributions to the radial current from the magnetic pre-sheaths and overestimates the total net radial current. But even this overestimated mobility was short of explaining the experimentally measured currents by about a factor of ten, after the effect of the toroidal acceleration of the neutrals by the rotating plasma was taken into account.

An expression for the orthogonal plasma conductivity, which is equivalent to expression (45) for the ion mobility, was originally derived by Boozer [33] for the core region of the plasma by averaging the momentum balance equation over the magnetic surface. Due to the toroidal momentum exchange between the SOL plasma and the target associated with the pressure asymmetry between the strike zones created by an externally applied radial electric field, this expression does not apply to the SOL.

The above considerations lead us to conclude that at least in the TdeV experiments described in [1], measured radial currents are probably of an anomalous nature, rather than a classical one. This, indeed, was the conclusion made in [1], based on the comparison between Eqs. (6) and (45), and experimentally measured scalings of ion mobility with toroidal field,

plasma current and plasma density. We strengthen this conclusion by stating that the magnitude of the classical contributions to the mobility is also too low to explain the experiment. We do not generalise our conclusions on anomalous mobility, confining it presently to the TdeV case, keeping in mind that different machines may operate in different regimes.

Finally, we wish to dispute a widespread opinion (reflected in [1], for example) that the dependence of the form (5) is one that originates from the "theory of damping through ion anomalous viscosity". One can easily demonstrate that the theory [12,13] does not require such a viscosity to obtain the scaling (5). It only requires Eq. (3) (which we have proven is wrong, however) and the assumption that strong pressure asymmetries between the targets are developed when $M_E \approx 1$, i.e. a radial electric field of the order of $c_s B_\theta$ (which is correct). By writing $\Delta p \sim p$ and substituting this into (3), we can obtain for the radial current density:

$$j_r \approx \frac{p}{2\pi a B} \ . \tag{47}$$

For $E_r \approx c_s B_\theta$ and the mobility defined according to (4), we obtain:

$$\mu \approx \frac{m c_s}{2\pi e a B_\theta B_\varphi} \ , \tag{48}$$

where we replaced p/n with mc_s^2. Similarity between this simple estimate and Eq. (5) becomes even closer, if we remember that (5) was derived in the double null geometry (poloidal pressure gradient divided by πa rather than by $2\pi a$ in our estimate for a single null configuration). Then, taking also into account the difference between c_s and v_i, our estimate would agree with Eq. (5) within 10%, excluding, of course, the unknown coefficient K. We must emphasise, however, that we do not agree with (3) as a valid equation for the net radial current. Our calculations of the current due to pressure gradient terms, performed in toroidal geometry, lead to Eq. (41), for the $\varepsilon = 0.33$ case, as an example. It gives a current 4-5 times smaller than that given by Eq. (47).

5.6 Effect of the B_T reversal on the radial ion flow

As was pointed out earlier (Section 5.4), in our model the direction of the radial current depends on the direction of the toroidal field, for a single null magnetic configuration. Due to toroidal effects, there should be an inward current for normal B_T, and an outward current for reversed B_T. In this sense the current originating from our model is different in principal from the one following from the theories of [7-10]. They do not require toroidal effects for the radial current, and the current does not depend on the direction of the toroidal field.

Due to its dependence on the direction of the toroidal field, the pressure gradient driven current and associated particle (ion) flow may offer an explanation for the well known

phenomenon of the dependence on the direction of the toroidal field on threshold power to cause the L-H transition. It has been observed, that in single null magnetic configuration, this threshold is lower for the "normal" (ion ∇B drift towards the target) B_T direction (see e.g. [34]). The current discussed in the present paper can make an impact on the edge transport which is in the "right" direction regarding the effect of the B_T direction on the L-H transition power threshold.

The inward direction of the ion flow in the "normal" field configuration, compared to an outward direction in the "reversed" field should improve both particle and energy confinement in the "normal" case, thus facilitating the L-H transition. We can make an estimate characterising the relative effect of the pressure gradient driven flow compared to anomalous diffusion. For the case of $\varepsilon = 0.33$, using the result (41), we can obtain:

$$\frac{j_r}{e\Gamma_{D_\perp}} = 0.22\frac{c_s\rho_s\lambda_{sol}}{2\pi a D_\perp} \ . \tag{49}$$

Using parameter F, introduced by Eq. (23), and the value $F \approx 0.185$, found in our calculations for $\varepsilon = 0.33$, the ratio (49) can be written as:

$$\frac{j_r}{e\Gamma_{D_\perp}} \approx 0.19\frac{\rho_{s\theta}}{\lambda_{sol}} \ . \tag{50}$$

In the conditions of $\rho_{s\theta} \approx \lambda_{sol}$, the ratio (50) can become quite high. Comparing total radial flows in the two opposite field directions, we can estimate their ratio as $(1+0.19)/(1-0.19) \approx 1.47$, which makes it a relatively strong effect.

5.7 Comparison with earlier theories of the dependence of the threshold power for the L-H transition on the B_T direction

Theories [24,25,29] have previously been proposed to explain the effect of the toroidal field direction on the power threshold for the L-H transition. It would be appropriate here to give brief summary of these theories and show the distinction between them and our model.

Models used in [24,25], as pointed out earlier in Section 5.1, share the same basis with our model in employing up-down asymmetries plus the toroidal effects of higher area and lower magnetic field on the outboard side, to get non-zero radial flows. These models analysed only heat flows through the separatrix, and found an extra ion heat pinch term in the "normal" field compared to the "reversed" field. An upper estimate for the ion heat flux can be easily obtained from the arguments preceding Eq. (40) as follows:

$$Q_{ir} = \frac{5}{2}\Gamma_{ir}T_i \approx \frac{5}{2}T_i n v_i \frac{\rho_i}{2\pi R} \ , \tag{51}$$

where $v_i = \sqrt{T_i/m}$ is the ion thermal velocity and ρ_i is the ion Larmor radius. Note that the equivalent ion particle flux, $Q_{ir}/(5/2 \cdot T_i)$, is smaller than the equivalent particle flux j_r/e following from estimate (40), when $T_i = T_e$, since only the ion component contributes to the ion heat flux. But it is very close to our numerical result (41) in the case of $\varepsilon = 0.33$.

A number of factors in [24,25] can, however, prevent the heat flux analysed there from reaching the upper limit (51). These theories combine standard neoclassical heat balance equations which are valid in the core, with an arbitrarily defined heat sink having a $-cos\theta$ dependence on the poloidal angle θ, to simulate the effect of the target. The complexity of the boundary separatrix layer involving sharp radial gradients of plasma density, temperature and parallel velocity, requiring the inclusion of extra terms from the viscous tensor, was ignored. These are exactly the problems that prohibit us from extending our model into the separatrix layer itself. In addition, these models can not be regarded as fully self-consistent, as they prescribe the poloidal dependence of the heat sink: $-cos\theta$. In the toroidal geometry any θ-dependence of the heat sink should follow from the model itself. Due to the influence of the target on the poloidal particle and heat fluxes (the target serves as a baffle), the poloidal dependence of the heat sink will be more complicated than just a $sin\theta$ and $cos\theta$ dependence.

The paper [29] considers particle and convective energy flows through the separatrix and finds an inward pinch term in the "normal" field compared to the outward flux in the "reversed" field. Being developed in cylindrical geometry, the theory [29] requires a certain mechanism that would create a temperature difference between the targets. The T_e asymmetry then leads to the appearance of the poloidal electric field and radial $\mathbf{E}\times\mathbf{B}$ drift. The model [29] employs a divertor geometry similar in the cross-section to the one used in the present paper. The assumption $T_i = T_e$ is also made. The poloidal dependence of the parallel heat flux was specified as:

$$q_{e\parallel} = \langle q_{e\parallel} \rangle + q_o \sin(\theta/2) \ , \tag{52}$$

where $\langle q_{e\parallel} \rangle$ is the poloidally constant heat flux, directed from the inner to the outer target (note that angles in [29] were defined differently from the ones adopted in the present paper and used in Eq. (52)). The second term is equal to $-q_o$ at the inner target (i.e. towards the target) and $+q_o$ at the outer target (also towards the target). Such an arbitrarily defined poloidal dependence of the heat flux was justified by the observation that the radial heat flow in the L-mode is the strongest on the outboard midplane, leading to power asymmetry between the targets in favour of the outer one.

After solving particle and heat balance equations, the surface averaged radial convective heat flux was obtained [29]:

$$\langle Q_r^{cl} \rangle \approx 5\alpha \frac{\chi_B}{\chi_{e\parallel}} \frac{B_\varphi}{B_\theta} \langle q_{e\parallel} \rangle \ , \tag{53}$$

where $\chi_B \equiv T_e/eB$, and $\alpha = 0.71$ for the pure Deuterium plasma. We can make an upper estimate of the equivalent particle flux $\langle \Gamma_r^{cl} \rangle = \langle Q_r^{cl} \rangle / 5T_e$. By assuming $\nabla_{||} T_e \approx T_e / 2\pi qR$ and substituting this temperature gradient in the heat flux $q_{e||} = -n\chi_{e||}\nabla_{||} T_e$, we obtain:

$$\langle \Gamma_r^{cl} \rangle \approx \frac{nc_s \rho_s}{4\pi a} \ . \tag{54}$$

This flux is of the same order as the equivalent particle flux following from (40) for practically important toroidicities ε.

Despite [29] claims to have identified fluxes through the separatrix, results strongly depend on the SOL physics. Extra terms in the viscosity tensor which are important in the boundary layer between the core and the SOL plasma have been neglected. In this respect [29] is in the same position as our model. One of the important differences between radial fluxes in [29] and the ones in our model, is that the fluxes in [29] are intrinsically ambipolar, while the pressure gradient driven current analysed in the present paper is carried only by the ions.

6. CONCLUSIONS

The simple model of the scrape-off layer in single null magnetic configuration, developed in this paper, includes effects of toroidal geometry and radial electric field. It predicts pressure asymmetry between the targets in favour of the outer one for the case of no radial electric field, and significant net radial currents. The direction of these currents depends on the direction of the toroidal magnetic field. The model also highlights some of the numerical problems of incorporating **E**×**B** drifts in 2D codes, work which is currently underway.

Despite being too simplistic principally in ignoring effects of neutrals on the SOL plasma, the model nevertheless seems to be able to answer two questions. The first is the question of whether the inclusion of the toroidal effects in a SOL model can result in a net radial current through the magnetic surface due to poloidal pressure variations. As it was shown, this current should be equal to zero in cylindrical geometry. Numerical calculations with self-consistent treatment of poloidal pressure variations have been performed, and results for the net radial current obtained. The current is non-zero for finite toroidicities, and its magnitude is consistent with simple estimates of the effects of up-down pressure asymmetry in toroidal geometry.

The second question is the dependence of the pressure gradient driven current on the externally applied radial electric field. This dependence was found to be very weak and non-monotonic against E_r. It is unlikely to explain the ion mobility derived from biasing experiments on TdeV, which, presumably, is strongly influenced by anomalous processes, not considered here. The magnitude of calculated radial current was not strongly affected by significant variations in poloidal pressure redistribution (due to the changes in the E_r). neutrals,

It was found that the direction of the pressure gradient driven current is inwards for the "normal" toroidal field (ion ∇B drift is towards the target) and outwards - for the "reversed" field. The current, carried by the ions, can significantly affect the particle flux in the scrape-off layer, when the SOL width approaches the ion poloidal Larmor radius. Therefore, it may be an explanation for the dependence of the power threshold for the L-H transition on the direction of the toroidal field. It is, however, unclear to what extent the currents obtained in the present SOL model can be extended to the separatrix layer. But, in this respect, our model is at least not in a worse position than previously offered explanations of the effect of the B_T direction on the L-H transition.

From the numerical calculations, it follows that the magnitude of the pressure gradient driven current scales as $j_r \sim \varepsilon^{\alpha}$, with $\alpha = 1.25 - 1.45$. This would imply that the beneficial effects of the "normal" direction of the toroidal field on confinement and the L-H transition power threshold increase with the increase in toroidicity.

ACKNOWLEDGEMENTS

The authors wish to thank Prof.K.Lackner for helpful discussions, Dr.M.J.Schaffer for critical comments and Prof.R.Weynants for particularly helpful discussions and for pointing out our previous neglect of the $V_{\perp}V_{\varphi}$ term in Eq. (12). PCS acknowledges support by the Canadian Fusion Fuels Technology Project.

REFERENCES

1. Lachambre J.-L., Quirion B., Boucher C. et al., Nucl. Fusion 34 (1994) 1431.
2. Staebler G.M., J. Nucl. Mater. 220-222 (1995) 158.
3. Stangeby P.C., Plasma Phys. and Contr. Fusion 37 (1995) 1337.
4. Günther K., 1995 Proc. 22nd Eur. Conf. on Contr. Fusion and Plasma Phys. (Bournemouth, 1995) vol 19C, part 1, p 433.
5. LaBombard B., Grossman A.A. and Conn R.W., J. Nucl. Mater. 176&177 (1990) 548.
6. Rognlien T.D., Milovich J.L., Rensink M.E. and Porter G.D., J. Nucl. Mater 196-198 (1992) 347.
7. Weynants R.R., Taylor R.J., Nucl. Fusion 30 (1990) 945.
8. Tsui H.Y.W., Phys. Fluids B 4 (1992) 4057.
9. Lingertat J., Günther K., Loarte A., J. Nucl. Mater. 220-222 (1995) 198.
10. Weynants R.R., Plasma Phys. and Contr. Fusion 37 (1995) 63.
11. Parks P.B., Nucl. Fusion 31 (1991) 373.
12. Rozhansky V., Tendler M., in: Proc. 20th Eur. Conf. on Contr. Fusion and Plasma Physics, Lisboa (1993) v.17 C, part 2, p.843.
13. Rozhansky V., Tendler M., Phys. Plasma 1 (1994) 2711.

14. Schaffer M.J. et al., submitted to Nucl. Fusion.
15. Baelmans M., Ph.D. thesis, Institute für Plasmaphysik Jül-2891 (1993).
16. Radford G.J. et al., presented at 5th Plasma Edge Theory Meeting, Asilomar, USA, 4-6 Dec., 1995, paper P-Mo5.
17. Chankin A.V., Stangeby P.C., Plasma Phys. and Contr. Fusion 36 (1994) 1485.
18. Stangeby P.C., McCracken G.M., Nucl. Fusion 30 (1990) 1225.
19. Liepmann H.W., Roshko A, in: "Elements of Gasdynamics", John Wily & Sons, Inc., New York - London (1957) p.48.
20. Harbour P.J., Loarte A., Nucl. Fusion 35 (1995) 759.
21. Stangeby P.C., Chankin A.V., Phys. Plasmas 2 (1995) 707.
22. Stangeby P.C., Chankin A.V., JET-P(95)07, submitted to Nucl. Fusion.
23. Tendler M., Rozhansky V., Comments Plasma Phys. Contr. Fusion 13 (1990) 191.
24. Hinton F.L., Nucl. Fusion 25 (1985) 1457.
25. Tang W.M., Hinton F.L., Nucl. Fusion 28 (1988) 443.
26. Chodura R., in: "Physics of Plasma-Wall Interaction in Controlled Fusion", Plenum Press, New York (1987) p.99.
27. Stangeby P.C., Plasma Phys. and Control. Fusion 33 (1991) 677.
28. Harbour P.J. and Loarte A., Contrib. Plasma Phys. 34 (1994) 2/3, 312.
29. Hinton F.L., Staebler G.M., Nucl. Fusion 29 (1989) 405.
30. Chankin A.V., Clement S., Erents K. et al., Plasma Phys. and Control. Fusion 36 (1994) 1853.
31. Chankin A.V., Campbell D.J., Clement S. et al., 1995 Proc. 22nd Eur. Conf. on Contr. Fusion and Plasma Phys. (Bournemouth, 1995) vol 19C, part 3, p 289.
32. Hutchinson I.H., LaBombard B., Goetz J.A. et al., Plasma Phys. and Contr. Fusion 37 (1995) 1389.
33. Boozer A.H., Phys. Fluids 19 (1976) 149.
34. Wagner F., Bartiromo R., Becker G. et al., Nucl. Fusion 25 (1985) 1490.

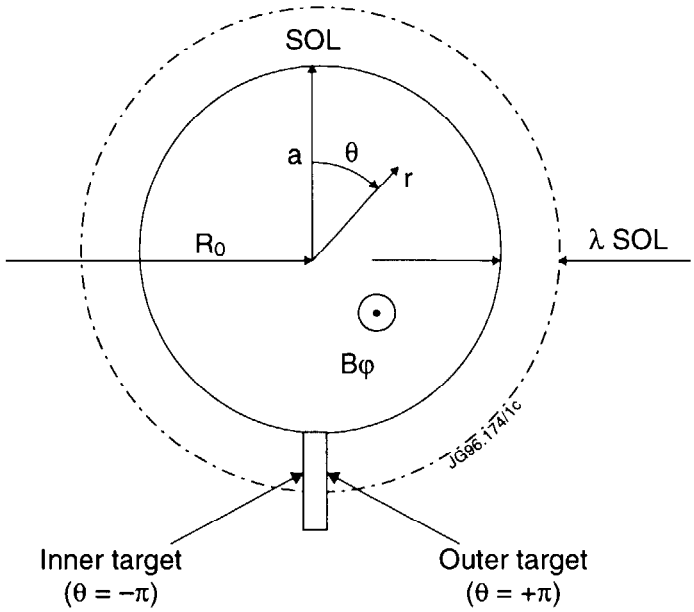

Fig.1 Geometry of the divertor model.

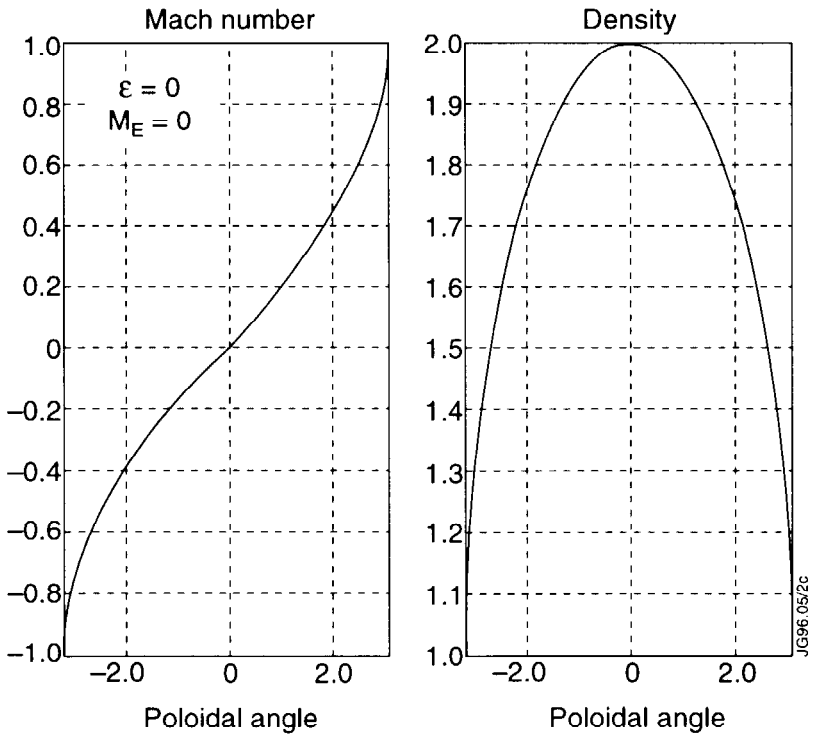

Fig.2 Mach number and density distributions for the cylindrical case ($\varepsilon = 0$) with zero electric field ($M_E = 0$). The density is normalised to be 1 at the inner target.

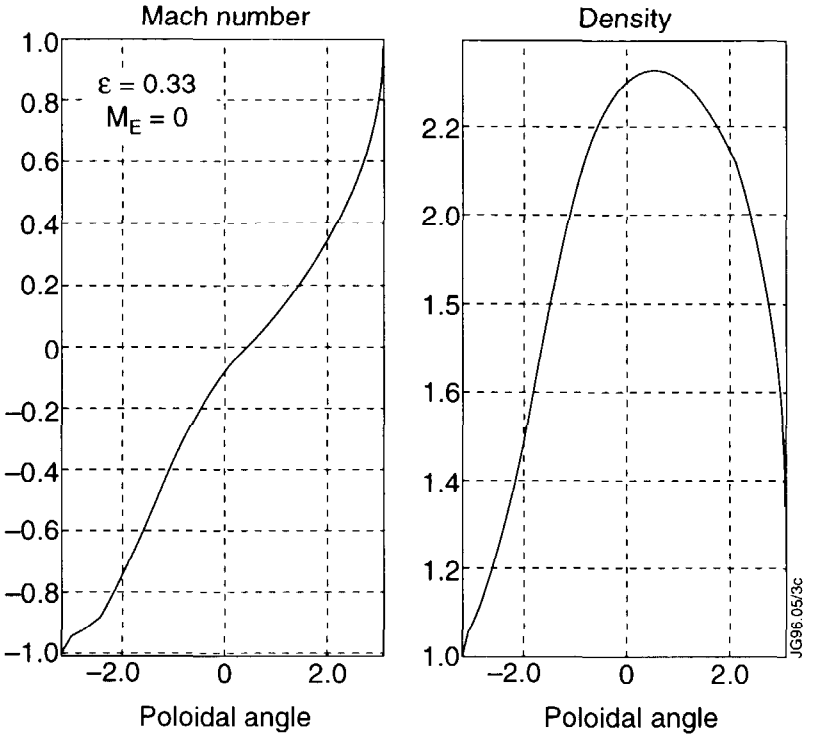

Fig.3 Mach number and density distributions for $\varepsilon = 0.33$ *and* $M_E = 0$. *The density is normalised to be 1 at the inner target.*

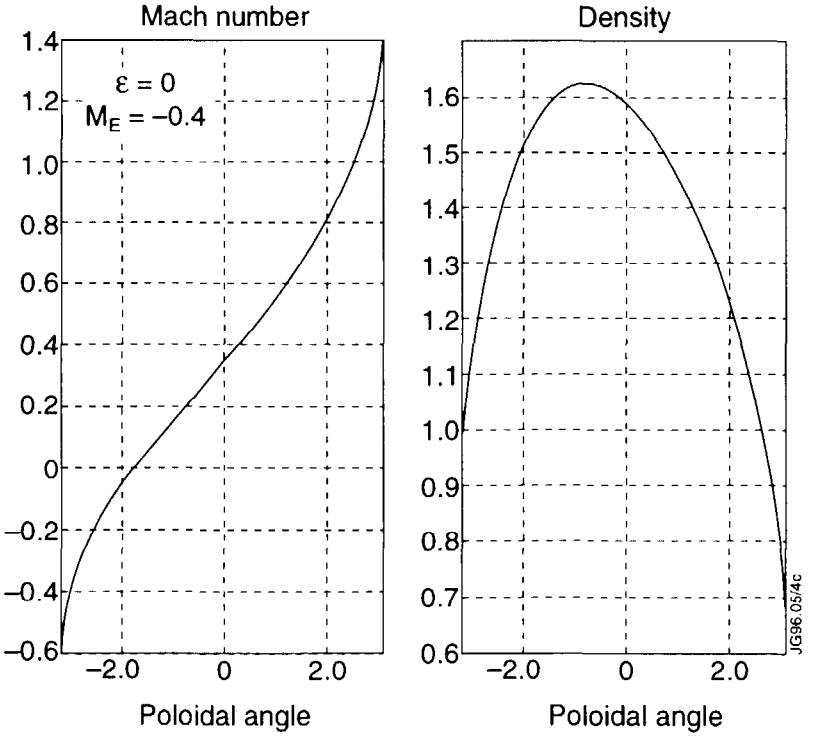

Fig.4 Mach number and density distributions for $\varepsilon = 0$ *and* $M_E = -0.4$. *The density is normalised to be 1 at the inner target.*

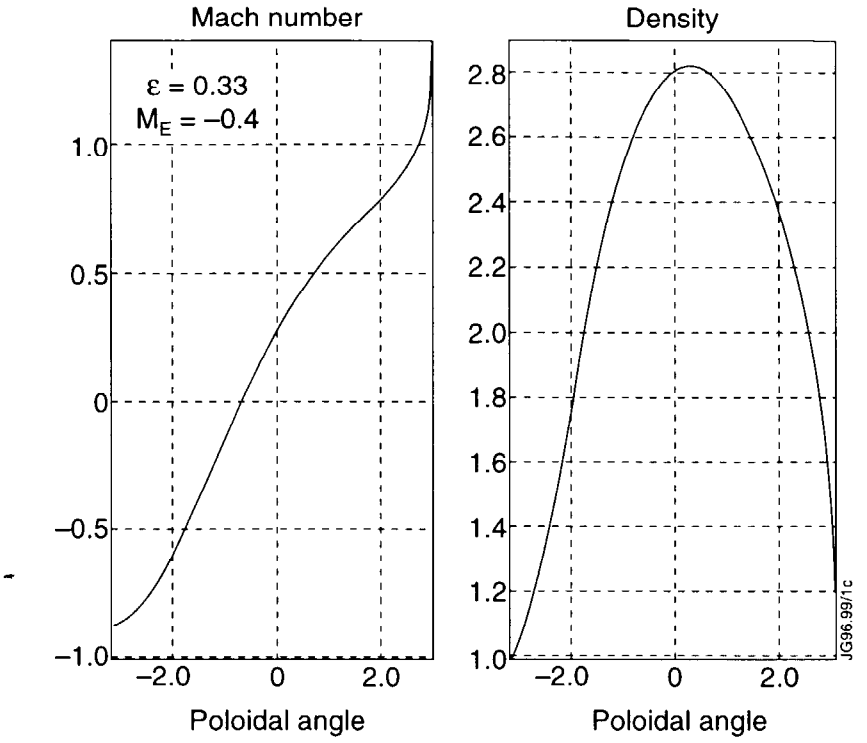

Fig.5 Mach number and density distributions for $\varepsilon = 0.33$ *and* $M_E = -0.4$. *The density is normalised to be 1 at the inner target.*

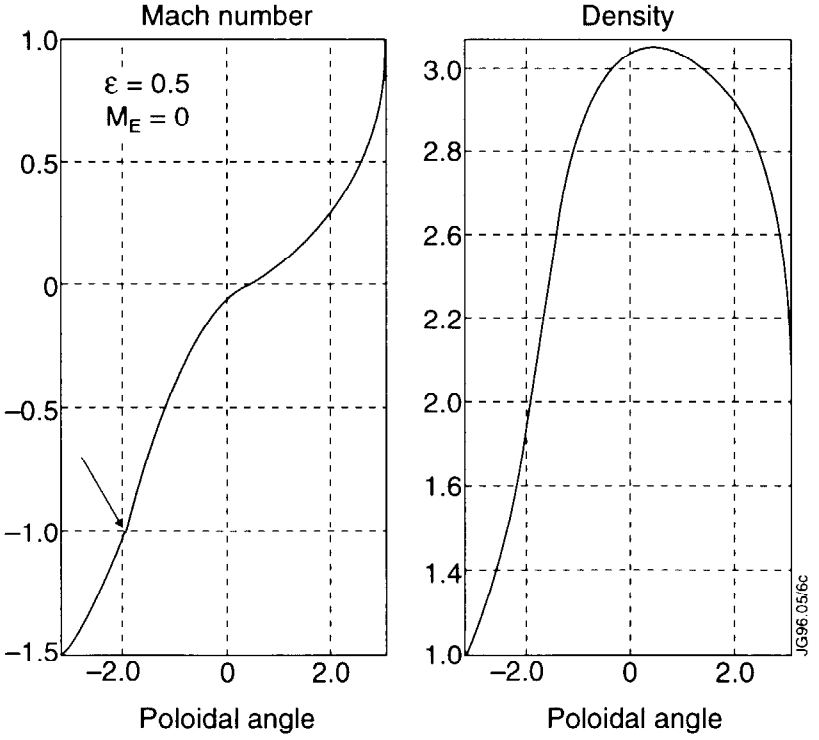

Fig.6 Mach number and density distributions for $\varepsilon = 0.5$ *and* $M_E = 0$. *The density is normalised to be 1 at the inner target.*

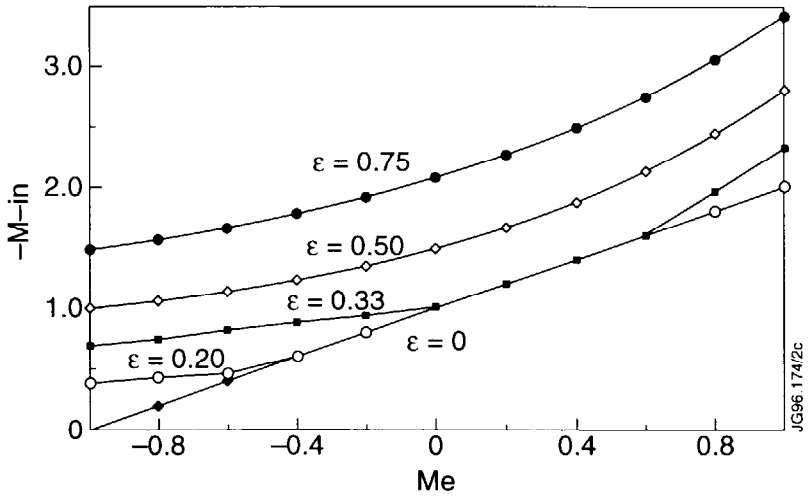

Fig.7 Mach number at the inner target ($-M$ is shown) for different ε *and* M_E. *The Mach number at the outer target always satisfied the "intuitive" boundary conditions:* $M|_{\theta=+\pi} = +1 - M_E$ *(Eq. (37)).*

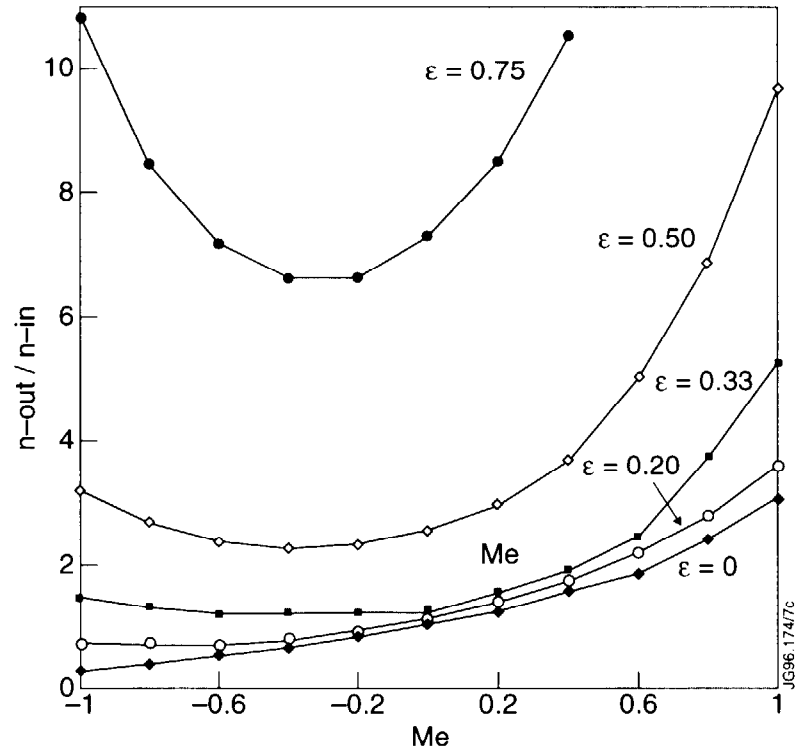

Fig.8 Density ratio between the targets, n_{out}/n_{in}, *as a function of* M_E *for different* ε.

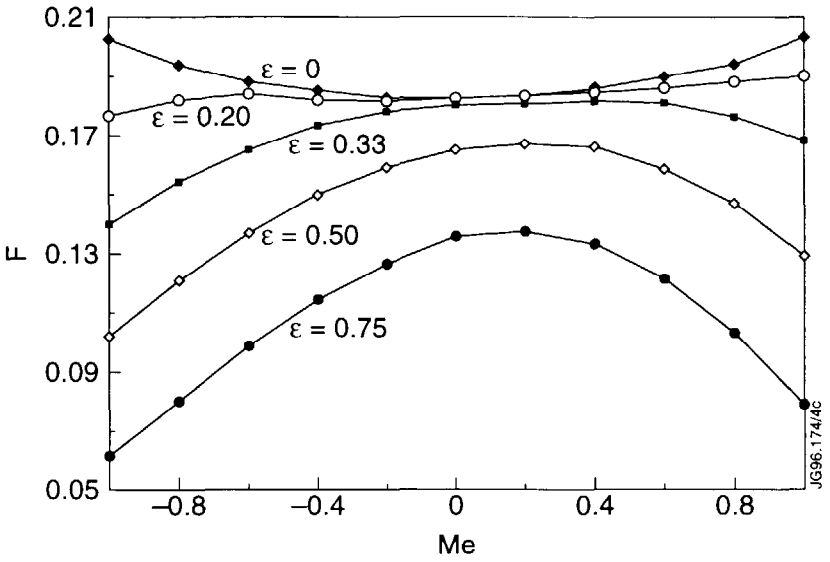

Fig.9 Eigenvalue F *as a function of* M_E *for different* ε.

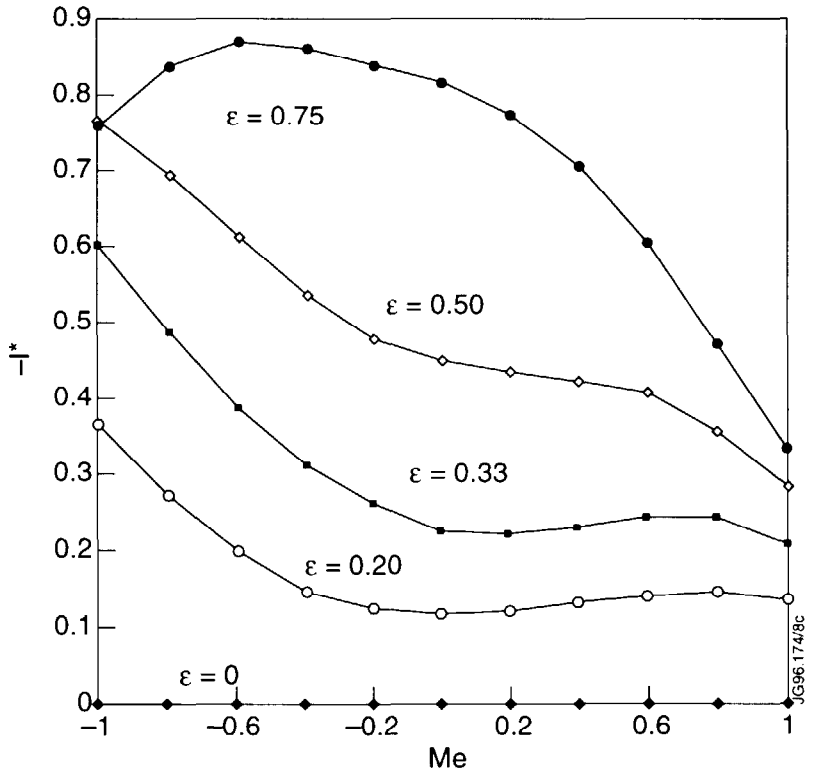

Fig.10 Normalised current ($-I^*$ *is shown) as a function of* M_E *for different* ε.

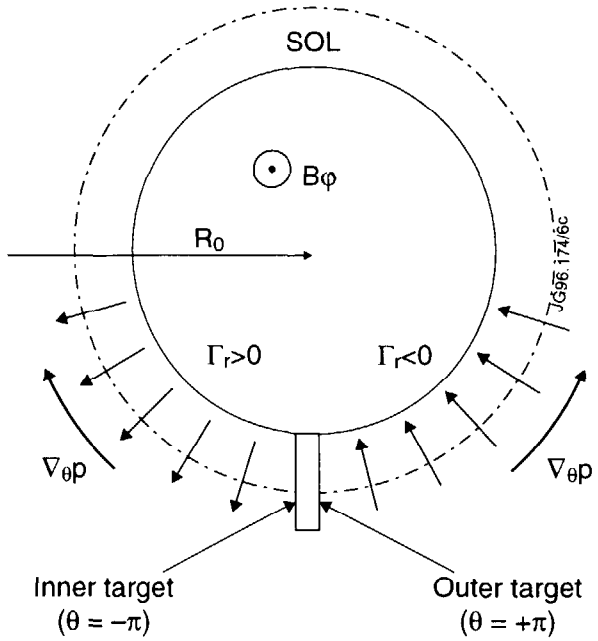

Fig.11 The origin of the pressure gradient driven current.

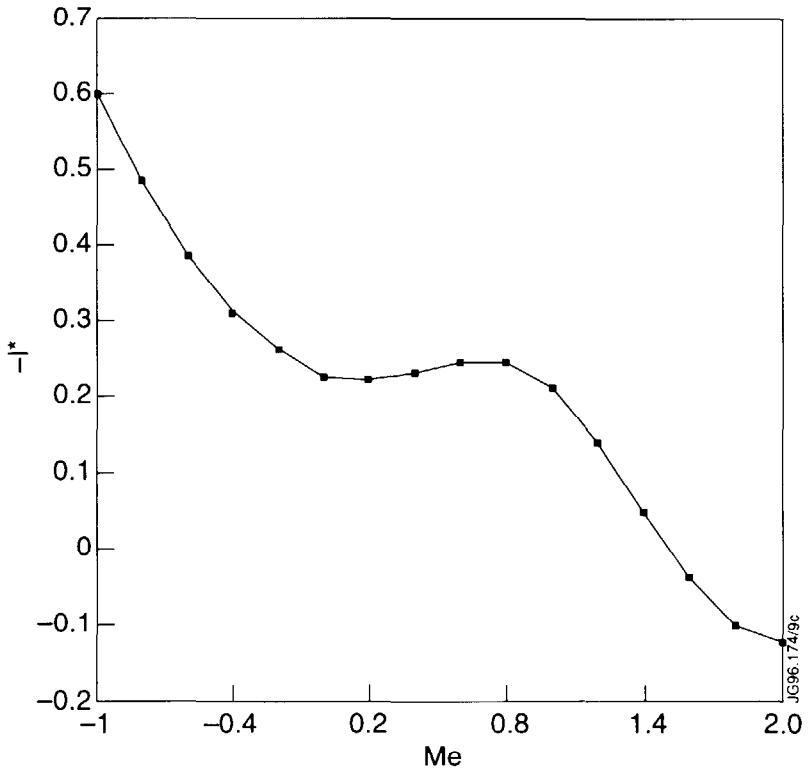

Fig.12 Normalised current ($-I^*$ is shown) as a function of M_E for the case of $\varepsilon = 0.33$.